Preprints.org

Article

Not peer-reviewed version

pH and Temperature-Dependent Dissolution Kinetics of Commercial Lightly-Burned Magnesia: Bridging Methodological Gaps for Cement Applications

Xiaowen Zhang and Juan Pablo Gevaudan *

Posted Date: 2 March 2026

doi: 10.20944/preprints202603.0128.v1

Keywords: lightly burned magnesia; MgO; dissolution kinetics; pH monitoring; alkaline conditions; aqueous chemistry; $Mg(OH)_2$ precipitation; magnesia-based cements

Preprints.org is a free multidisciplinary platform providing preprint service that is dedicated to making early versions of research outputs permanently available and citable. Preprints posted at Preprints.org appear in Web of Science, Crossref, Google Scholar, Scilit, Europe PMC.

Copyright: This open access article is published under a Creative Commons CC BY 4.0 license, which permit the free download, distribution, and reuse, provided that the author and preprint are cited in any reuse.

Preprints.org (www.preprints.org) | NOT PEER-REVIEWED | Posted: 2 March 2026 doi:10.20944/preprints202603.0128.v1

Disclaimer/Publisher's Note: The statements, opinions, and data contained in all publications are solely those of the individual author(s) and contributor(s) and not of MDPI and/or the editor(s). MDPI and/or the editor(s) disclaim responsibility for any injury to people or property resulting from any ideas, methods, instructions, or products referred to in the content.

Article

pH and Temperature-Dependent Dissolution Kinetics of Commercial Lightly-Burned Magnesia: Bridging Methodological Gaps for Cement Applications

Xiaowen Zhang [1] and Juan Pablo Gevaudan [2,3,*]

[1] Fiber and Particle Engineering Research Unit, University of Oulu, Pentti Kaiteran katu 1, 90570 Oulu, Finland
[2] Department of Architectural Engineering, The Pennsylvania State University, University Park, PA, 16802, USA
[3] Department of Materials Science and Engineering, The Pennsylvania State University, University Park, PA, 16802, USA
* Correspondence: j.p.gevaudan@psu.edu

Abstract

Performance variability in MgO-based cements stems partly from poorly characterized dissolution kinetics of commercial lightly burned magnesia (LBM). Existing studies focus on high-purity materials under acidic conditions, but LBM dissolves also in alkaline condition where $Mg(OH)_2$ precipitation prevents reliable sampling at high pH. We validated pH monitoring against ICP-AES for tracking initial LBM dissolution kinetics across pH 2.0-11.0 and temperatures 25-85°C. Commercial LBM (32 m^2/g, 7.5 wt% CaO) exhibited rates one to two orders of magnitude higher than synthetic magnesia (10^{-8} to 10^{-12} $mol/cm^2 \cdot s$). X-ray diffraction, electron microscopy with energy-dispersive spectroscopy, and BET analysis revealed enhanced reactivity from poor crystallinity, multiphase composition, and high surface area with textural porosity. Temperature effects peaked at 75°C before declining due to $Mg(OH)_2$ passivation. The validated method provides practical guidance for MBC quality control and performance optimization.

Keywords: lightly burned magnesia; MgO; dissolution kinetics; pH monitoring; alkaline conditions; aqueous chemistry; Mg(OH)2 precipitation; magnesia-based cements

1. Introduction

Magnesia-based cements (MBCs) have emerged as promising low-carbon alternatives to Portland cement, owing to their lower calcination temperatures and the potential for direct CO_2 sequestration through mineral carbonation [1,2]. However, industrial adoption remains constrained by significant performance variability, particularly in setting behavior, early-age strength development, and long-term durability. Understanding the fundamental dissolution mechanisms controlling this variability is essential for advancing MBC technology from laboratory demonstrations to reliable construction materials.

Unlike Portland cement systems where tricalcium silicate hydration dominates, MBC strength development depends critically on the initial dissolution of magnesia (MgO) to provide Mg^{2+} ions for subsequent reactions with supplementary components, forming binding phases such as magnesium silicate hydrate (M-S-H) or hydrotalcite-like phases [3–5]. Although MgO dissolution has been scrutinized for decades, the published kinetic data show significant discrepancies. Reported rates can differ by as much as four orders of magnitude even when experimental conditions are nominally identical [6–9]. This variability cannot be attributed solely to experimental methodology differences and instead points to fundamental material-dependent factors that remain poorly understood.

The discrepancy becomes particularly relevant when considering that commercial MBCs utilize lightly-burned magnesia (LBM), produced by calcining natural magnesite or brucite at relatively low temperatures (700-1000°C) [10]. This production route yields materials with characteristics distinctly

© 2026 by the author(s). Distributed under a Creative Commons CC BY license.

Preprints.org (www.preprints.org) | NOT PEER-REVIEWED | Posted: 2 March 2026 doi:10.20944/preprints202603.0128.v1

different from the high-purity MgO crystals or dead-burned magnesia commonly employed in fundamental dissolution studies. Commercial LBM is characterized by higher specific surface areas (typically 20-50 m^2/g), variable crystallinity arising from incomplete thermal transformation, and significant levels of calcium, silicon, iron, and aluminum impurities inherited from natural feedstocks [11–13]. Previous studies have suggested that surface defects, lattice disorder, and impurity incorporation can significantly affect oxide dissolution rates [14–16], with dopants and calcium-bearing phases potentially creating preferential dissolution sites [17,18]. Recent work has revealed that LBM reactivity depends on synergistic effects between mesoporous pore networks that facilitate water transport and surface oxygen vacancy concentrations that promote hydrolysis [19], challenging the conventional assumption that specific surface area alone determines reactivity. However, these mechanistic insights have been derived primarily from hydration tests in pure water, and the dissolution behavior across the wide pH spectrum encountered during actual MBC formulation and curing remains largely uncharacterized [20]. This knowledge gap hinders efforts to standardize LBM quality or predict MBC performance from precursor characteristics.

A critical methodological limitation further restricts our understanding of MgO dissolution under cement-relevant conditions. Most fundamental studies are conducted in acidic environments to maintain stoichiometric dissolution and avoid secondary phase precipitation. However, MBC systems operate across a buffered alkaline spectrum, typically ranging from the initial hydrolysis of MgO near pH 10 to the higher alkalinity of mature hydration environments. Under these alkaline conditions, the low solubility of $Mg(OH)_2$ ($K_{sp} = 5.61 \times 10^{-12}$) [21] and its rapid precipitation kinetics establish a dynamic dissolution-precipitation equilibrium that precludes accurate sampling-based measurements [8,22]. Quantifying dissolved Mg2+ concentrations via inductively coupled plasma spectrometry (ICP) is inherently problematic at pH > 8 because of the inevitable precipitation during sample preparation and analysis. Consequently, the field lacks a validated analytical framework for tracking MgO consumption continuously across the full pH range relevant to cement hydration.

This study addresses these interconnected material and methodological gaps by investigating the dissolution behavior of a representative commercial LBM across a pH range of 2.0 to 11.0 and temperatures from 25 to 85°C. These conditions encompass the entire spectrum from initial mixing to accelerated curing. Our primary objective is to validate pH monitoring as a practical and continuous method for determining dissolution rates, particularly in alkaline regimes where precipitation makes direct ionic measurement impractical. We evaluate pH-derived rates against ICP-AES measurements where feasible. Simultaneously, we employ comprehensive material characterization, including X-ray diffraction, scanning and transmission electron microscopy, and surface area analysis, to identify the physicochemical properties that distinguish commercial LBM from synthetic reference materials and drive its dissolution kinetics. By establishing quantitative structure-kinetics relationships, this work provides practical guidance for MBC formulation design, quality control protocols, and the optimization of curing conditions to ensure predictable performance.

2. Materials and Methods

2.1. Materials

The lightly burned magnesia used in this study was a commercial product (MagOx XL, Premier Magnesia, LLC, Waynesville, NC), representative of materials commonly employed in MBC formulations. This LBM is produced by calcination of natural magnesite at temperatures below 1000°C, resulting in a reactive magnesia with characteristic impurities from the parent ore. For comparison, a high-purity synthetic magnesia (STM) was obtained from ThermoFisher Scientific Chemicals (99.99% purity). The chemical compositions and specific surface areas of both materials are presented in **Table 1**.

© 2026 by the author(s). Distributed under a Creative Commons CC BY license.

Preprints.org (www.preprints.org) | NOT PEER-REVIEWED | Posted: 2 March 2026 doi:10.20944/preprints202603.0128.v1

Table 1. Chemical composition and BET-specific surface area of lightly burned and synthetic MgO.

Raw material	Oxide content (%)					SSA (m^2/g)
	MgO	SiO_2	Fe_2O_3	Al_2O_3	CaO	
Lightly Burned MgO (LBM)	87.8	3.18	0.91	0.34	7.50	32.3
Synthetic MgO (STM)	99.99	0.01	ND	ND	ND	10.1

The substantial differences in impurity content and surface area between these materials provide an ideal system for investigating the effects of material properties on dissolution kinetics. The LBM contains significant levels of CaO (7.5 wt%) and SiO_2 (3.18 wt%), which are typical of commercial materials derived from natural sources. Note that while the manufacturer's safety data sheet reports 93% MgO and 3% CaO, more detailed characterization by X-ray fluorescence revealed the complete composition shown in **Table** All dissolution experiments utilized deionized water (resistivity >17 MΩ·cm) and ACS-grade reagents including hydrochloric acid (HCl), nitric acid (HNO_3), sulfuric acid (H_2SO_4) and sodium hydroxide (NaOH) for pH adjustment.

2.2. Material Characterization

Scanning electron microscopy was performed to examine the morphological differences between LBM and STM. Powder samples were mounted on aluminum stubs using conductive carbon tape and sputter-coated with gold (<5 nm thickness) to prevent charging. Images were acquired using a field emission SEM operated at accelerating voltages of 5-15 kV and beam current of 50 pA.

X-ray diffraction patterns were collected to assess crystallinity and phase composition. Powders were front-loaded into silicon zero-background holders and analyzed using an Empyrean diffractometer (Malvern Panalytical) equipped with Cu Kα radiation (λ = 1.5406 Å) operated at 45 kV and 40 mA. Diffraction data were collected from 5° to 80° 2θ with a step size of 0.026° and counting time of 150 seconds per step. The incident beam path included Bragg-Brentano HD optics with 0.04 radian Soller slits and a 1/4° fixed divergence slit. Phase identification was performed using Jade software (version 8.9, MDI) with the ICDD PDF-5 database. Peak broadening analysis was conducted on the (200) reflection of periclase to estimate crystallite size using the Scherrer equation after correction for instrumental broadening.

BET surface area measurements were performed using nitrogen adsorption at 77 K on a Micromeritics ASAP 2020 analyzer. Samples were degassed at 200°C for 4 hours under vacuum prior to analysis. Pore size distributions were calculated from the desorption branch using the Barrett-Joyner-Halenda method.

We further investigated the nanoscale structure and chemical distribution of the precursors using scanning transmission electron microscopy (STEM). The analysis was performed on a Talos F200X microscope operated at 200 kV. High-angle annular dark-field (HAADF) images were acquired to observe mass-thickness contrast and generated corresponding energy-dispersive X-ray spectroscopy (EDS) maps to visualize the spatial distribution of key elements.

2.3. Dissolution Experiments

Dissolution kinetics were characterized using an automated reactor system (EasyMax 102, Mettler Toledo) capable of precise thermal regulation (±0.1°C). For each experiment, 400 mL of solution was adjusted to an initial pH between 2.0 and 11.0 using appropriate acids or bases and equilibrated to the target temperature (25, 35, 45, 75, or 85°C). Upon reaching thermal equilibrium, 100 mg of MgO powder was introduced to the solution, yielding a low solid-to-liquid ratio (0.25 g/L). This dosage was selected to minimize bulk pH drift while ensuring sufficient sensitivity for tracking ion release under the alkaline conditions typical of magnesia-based cements. All dissolution tests were conducted under quiescent (non-stirred) conditions. This approach was adopted to mitigate experimental artifacts associated with

© 2026 by the author(s). Distributed under a Creative Commons CC BY license.

Preprints.org (www.preprints.org) | NOT PEER-REVIEWED | Posted: 2 March 2026 doi:10.20944/preprints202603.0128.v1

mechanical stirring, such as particle aggregation and wall adhesion, which inconsistently reduce the effective reactive surface area. By utilizing a standardized cylindrical vessel (80 mm internal diameter, 100 mm depth) and maintaining a constant solution volume, we ensured a reproducible diffusion boundary layer for all samples. This static setup also serves as a reasonable proxy for the low-convection environment inherent in fresh cement pastes. To ensure data fidelity, the pH electrode (InLab Expert, Mettler Toledo) was fixed at the vessel centerline, 30 mm below the liquid surface, with measurements logged at 5-second intervals. The electrode underwent a three-point calibration (pH 4.01, 7.00, and 10.01) every 4 hours to account for potential drift and ensure long-term stability.

For comparison with LBM, selected experiments used high-purity synthetic magnesia (STM, see Section 2.1) under identical conditions to validate that the observed dissolution behavior reflects material-specific properties rather than methodological artifacts.

2.4. Dissolution Rate Determination

Two complementary methods were employed to determine dissolution rates. The primary approach utilized pH monitoring to calculate MgO consumption based on stoichiometric flux analysis.

In acidic conditions (pH < 8), the dissolution is primarily driven by proton consumption ($MgO + 2H^+ \rightarrow Mg^{2+} + H_2O$). By measuring pH over time, the rate of proton consumption can be calculated in moles per unit volume ($\Delta[H^+] = 10^{-pH_{(t=0)}} - 10^{-pH_{(t=x)}}$, in mol/L). Utilizing the molar ratios from the hydration reaction and the solution volume (V_R, 400ml), the fraction of dissolved MgO ($X = m_{dissolved,\ MgO}/m^0_{MgO}$) can be represented as:

$$10^{-pH^0} - 10^{-pH} = \frac{2m^0_{MgO}}{V_R M_{MgO}} X \quad (1)$$

where M_{MgO} is the molar mass (40.3 g/mol), m_{MgO} is the initial mass of MgO added to the reaction (mg, 100mg). Assuming constant surface area (S) during the initial phase, the dissolution rate (r, in $mol \cdot cm^{-2} \cdot s^{-1}$) is derived from the linear slope of proton consumption:

$$10^{-pH^0} - 10^{-pH} = \frac{2rS}{V_R} t \quad (2)$$

where V_R is the solution volume (0.40 L) and S is the total surface area (cm^2) derived from BET analysis.

Under alkaline conditions (pH > 8), MgO dissolution proceeds via the direct hydration reaction ($MgO + H_2O \rightarrow Mg^{2+} + 2OH^-$). In this regime, the rate was determined by tracking the production of hydroxide ions:

$$[OH^-]_t - [OH^-]_0 = \frac{2rS}{V_R} t \quad (3)$$

where $[OH^-]_t$ and $[OH^-]_0$ represent the measured and initial hydroxide concentrations, respectively, and other terms are as defined previously.

Linear regression was performed on the kinetic data within the initial 5 seconds of the reaction. This interval was selected as the process exhibited a linear relationship characteristic of surface-controlled mechanisms before significant diffusion limitations or, at high pH, precipitation effects occurred. The short measurement window ensures that reported rates represent true dissolution kinetics rather than dissolution-precipitation equilibrium, which is particularly important at pH >9 where $Mg(OH)_2$ precipitation is thermodynamically favorable. The slopes from these regressions were used to calculate the specific dissolution rate r. For the multiphase LBM, this calculated rate represents the effective release of hydroxide ions from the bulk material, providing a practical index of reactivity for cement formulation.

To independently validate the stoichiometric pH-based calculations, the dissolution rate was also calculated directly from the magnesium ion concentration measured via ICP-AES:

$$r = \frac{[Mg^{2+}] \cdot V_R}{S \cdot t} \quad (4)$$

This method provides a direct quantification of mass transfer without assumptions regarding surface speciation or proton consumption stoichiometry.

© 2026 by the author(s). Distributed under a Creative Commons CC BY license.

Preprints.org (www.preprints.org) | NOT PEER-REVIEWED | Posted: 2 March 2026 doi:10.20944/preprints202603.0128.v1

2.5. Aqueous Sampling and ICP-AES Analysis

Selected experiments included direct determination of dissolved magnesium to validate the pH-based measurements. Aliquots were collected using both automated sampling (EasySampler, Mettler Toledo) and manual syringe sampling. The automated system withdrew 20 µL samples at 2.86-minute intervals from a consistent depth of 2 cm below the solution surface. Manual sampling using 5 mL syringes provided additional time points at 1, 2, 3, 4, and 5 minutes to capture initial kinetics. All samples were immediately filtered through 0.45 µm PTFE syringe filters to remove suspended particles. Filtered samples were diluted 1:10 with 2% HNO_3 (trace metal grade) to stabilize dissolved species and prevent precipitation. Magnesium concentrations were determined by inductively coupled plasma atomic emission spectroscopy (ICP-AES) within 24 hours of collection, with most samples analyzed within 4-6 hours. The instrument was calibrated using matrix-matched standards with detection limits of 0.01 mg/L and analytical precision better than 2% RSD.

3. Results and Discussions

3.1. Precursor Characteristics

As in section 2.1, **Table 1** highlights distinct compositional and microstructural differences between the two precursors. Commercial LBM contains significant impurities (7.5 wt% CaO, 3.18 wt% SiO_2) and possesses a specific surface area (SSA) of 32.3 m^2/g, whereas STM is analytically pure with a lower SSA of 10.1 m^2/g.

SEM imaging (**Figure 1**) links the threefold SSA disparity to particle texture. STM (**Figure 1a–b**) appears as dense, monolithic particles with smooth cleavage surfaces. In contrast, LBM (**Figure 1c–d**) consists of hierarchical aggregates of primary nanoparticles, creating a rough, open texture.

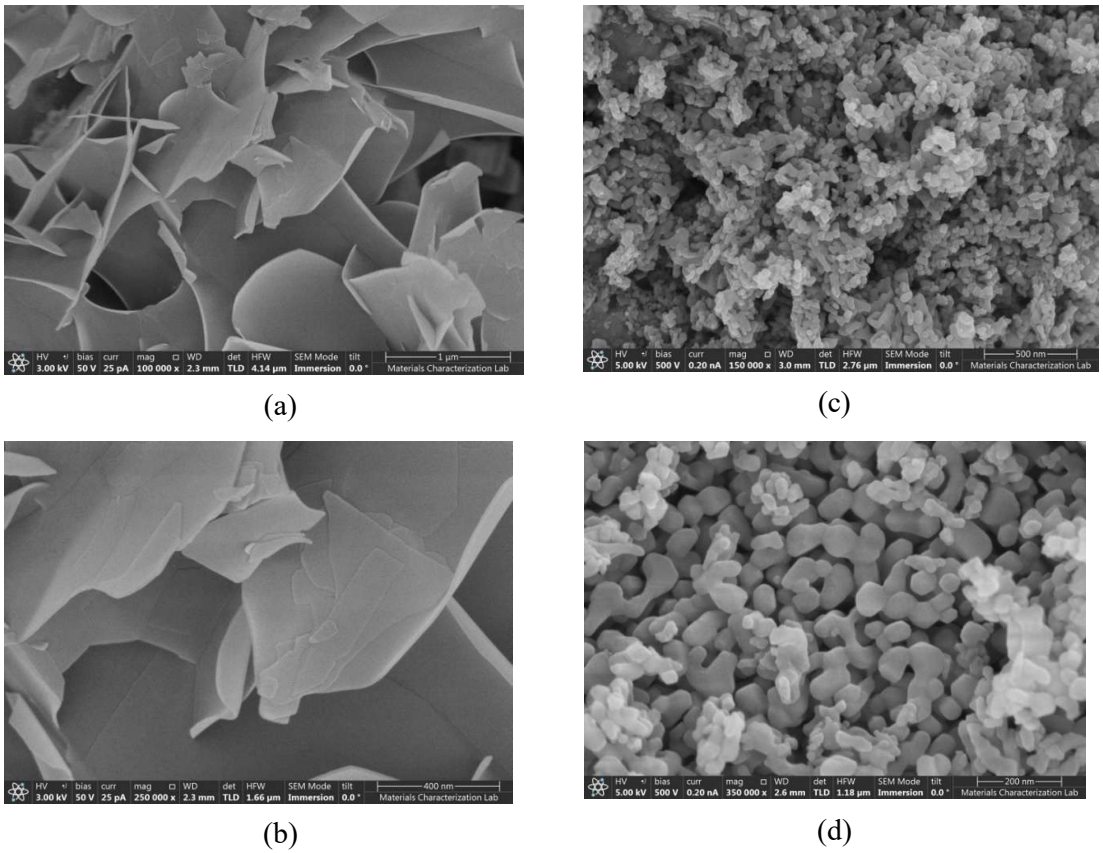

Figure 1. SEM images for analytically pure STM (a), (b); and commercial LBM (c), (d) as utilized in this study.

© 2026 by the author(s). Distributed under a Creative Commons CC BY license.

Preprints.org (www.preprints.org) | NOT PEER-REVIEWED | Posted: 2 March 2026 doi:10.20944/preprints202603.0128.v1

TEM analysis (**Figure 2**) supports this observation; STM displays sharp, faceted terminations (**Figure 2c–d**) indicative of high crystallinity, while LBM particles exhibit diffuse, irregular boundaries (**Figure 2a–b**). These features confirm that the elevated SSA of LBM arises from external roughness and particle aggregation rather than a well-defined internal pore network.

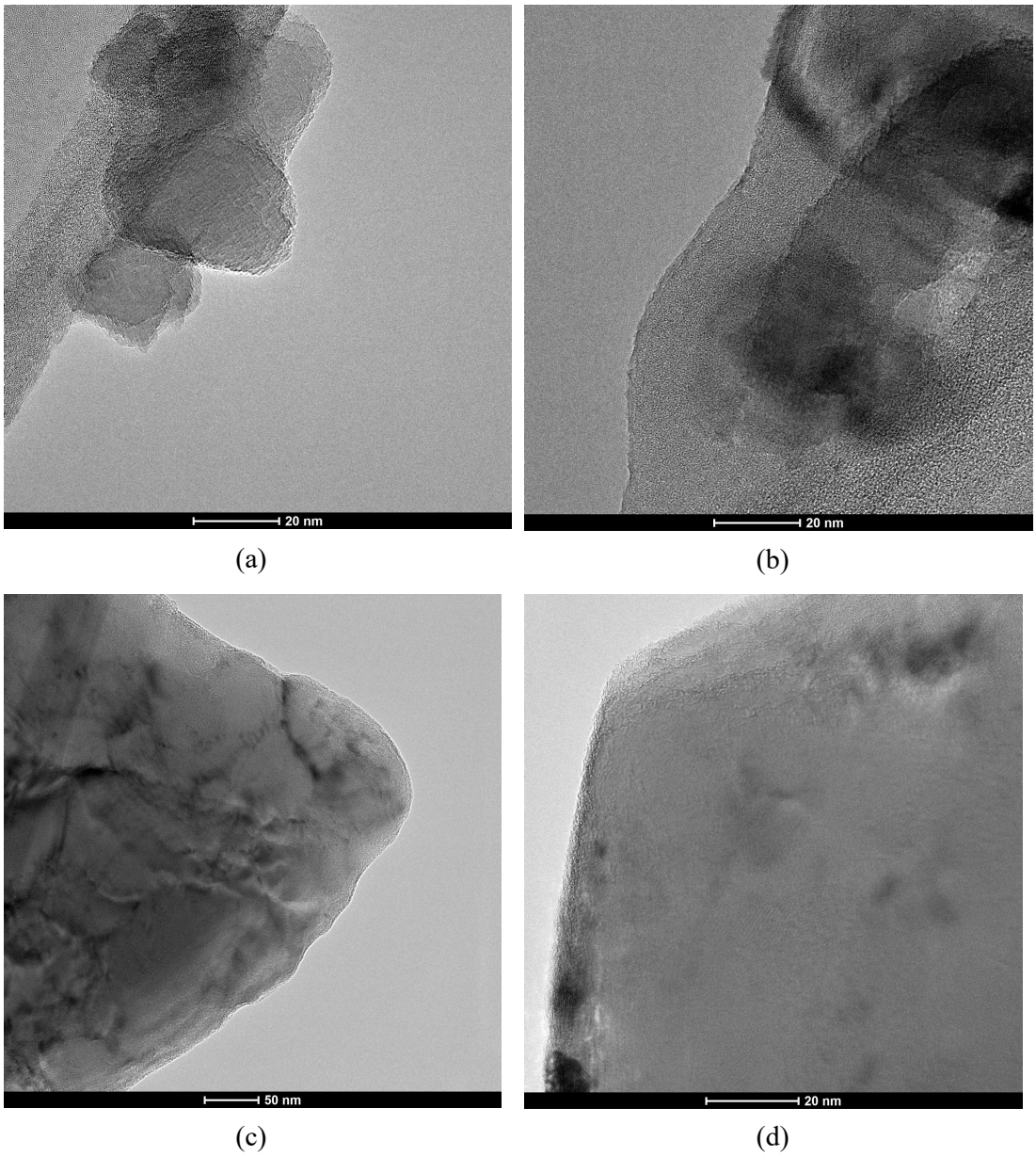

Figure 2. TEM morphology images of LBM (a), (b) and STM (c), (d), with scales 20 nm and 50 nm.

Notably, the dissolution kinetics (**Section 3.2**) demonstrate that LBM exhibits a significantly higher reaction rate than STM even after normalizing for specific surface area. This implies that the intrinsic reactivity per unit surface area of LBM is superior. XRD profiles (**Figure 3**) provide the crystallographic evidence for this enhancement. Unlike the sharp, high-intensity periclase peaks of STM (**Figure 3b**), the LBM patterns (**Figure 3a**) show broadened reflections and a complex assemblage of minor phases, including quartz (Q), forsterite (F), and calcite (L). The observed peak broadening in the periclase phase is consistent with reduced crystallite size and lattice microstrain, pointing to a higher density of surface defects (e.g., steps and vacancies) that serve as thermodynamically active sites for dissolution.

© 2026 by the author(s). Distributed under a Creative Commons CC BY license.

Preprints.org (www.preprints.org) | NOT PEER-REVIEWED | Posted: 2 March 2026 doi:10.20944/preprints202603.0128.v1

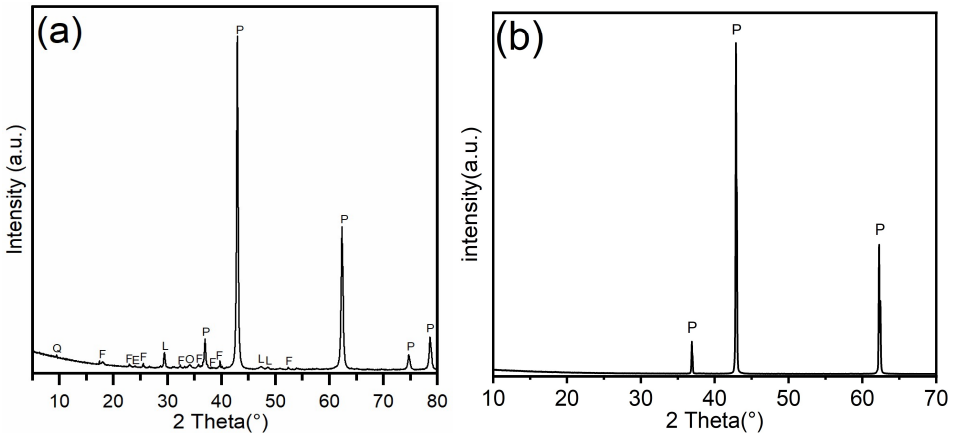

Figure 3. XRD patterns of (a) lightly burned magnesia, (b) synthetic magnesia. The lightly burned magnesia contains: quartz, Q (PDF# 010-090-3640); forsterite, F (PDF# 04-008-7944); hematite, E (PDF# 04-008-8479); calcite, L (PDF#98-000-0141); portlandite, O (PDF# 04-027-9358); and periclase, P (PDF# 00-004-0829). The synthetic magnesia contains: periclase, P (PDF# 00-004-0829).

Complementary high-angle annular dark-field (HAADF) STEM and EDS mapping (**Figure 4**) reveal a decisive chemical contrast. STM (**Figure 4b**) shows a uniform distribution of Mg and O. Conversely, LBM (**Figure 4a**) exhibits nanoscale segregation, where Ca and Si impurities appear as localized clusters rather than a uniform solid solution. These domains correspond to the minor phases (e.g., calcite, silicates) identified in XRD. The interfaces between these impurity phases and the MgO matrix likely create boundaries of mismatched solubility. Preferential leaching of these more soluble domains may generate local initiation points for dissolution, providing a secondary kinetic pathway absent in the chemically homogeneous STM.

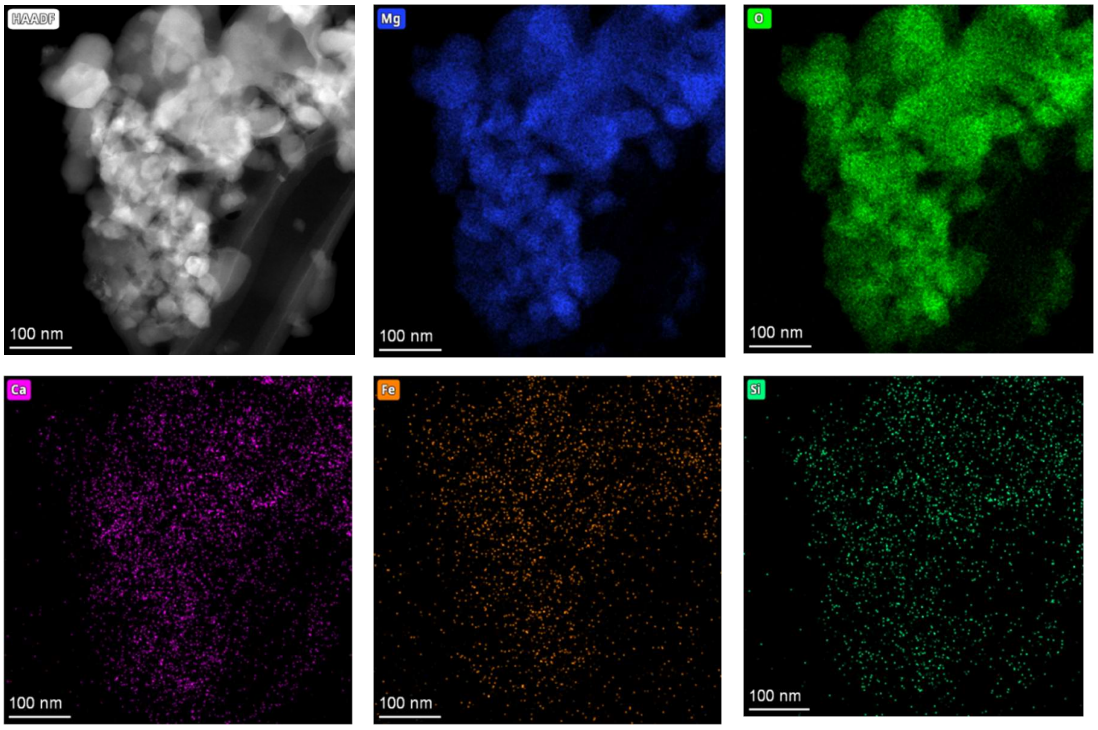

(a)

© 2026 by the author(s). Distributed under a Creative Commons CC BY license.

Preprints.org (www.preprints.org) | NOT PEER-REVIEWED | Posted: 2 March 2026 doi:10.20944/preprints202603.0128.v1

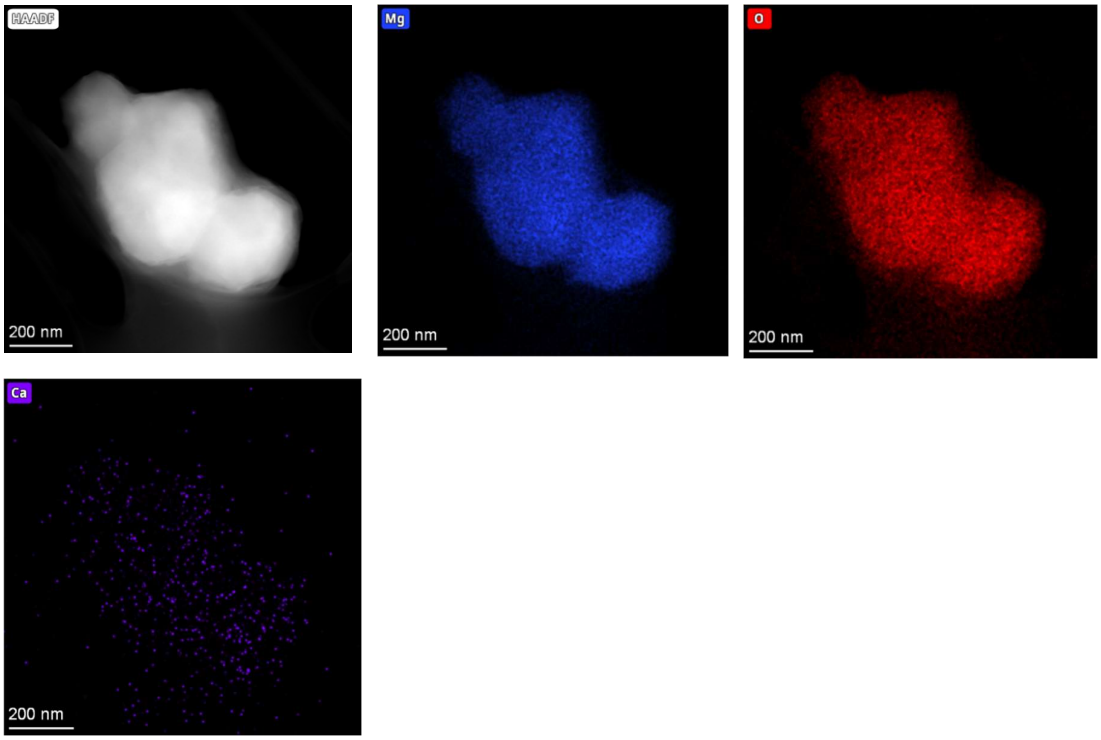

(b)

Figure 4. HAADF-STEM images and EDS maps for LBM (a) showing elemental distribution (blue Mg, green O, purple Ca, orange Fe, cyan Si) and for STM (b) showing uniform Mg (blue) and O (red).

3.2. Comparative Dissolution Kinetics of LBM and STM

To quantify the impact of the physicochemical differences identified in **Section 3.1**, dissolution kinetics of LBM were benchmarked against high-purity synthetic magnesia (STM) at 25°C and 35°C under near-neutral conditions. As shown in **Figure 5**, both materials exhibit an instantaneous, near-vertical pH rise within the first seconds, confirming that rapid surface hydroxylation is intrinsic to both commercial and synthetic magnesia. STM follows a smooth progression toward equilibrium, consistent with the dissolution of a homogeneous, single-phase solid. In contrast, LBM displays a distinct non-monotonic profile characterized by an initial overshoot and subsequent fluctuations between 200 and 500 seconds before recovering and ascending to a final equilibrium that exceeds the initial peak. This indicates a dynamic competition between rapid ion release from reactive impurities and transient surface precipitation events, resulting in higher equilibrium values (10.5-11.0 for LBM vs. 9.5-10.0 for STM).

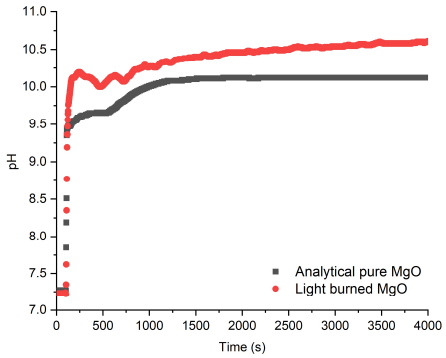

Figure 5. Comparative dissolution behavior of analytical pure STM and commercial LBM in aqueous solutions at 25 °C. In general, all samples exhibited similar logarithmic pH rise over time.

© 2026 by the author(s). Distributed under a Creative Commons CC BY license.

Preprints.org (www.preprints.org) | NOT PEER-REVIEWED | Posted: 2 March 2026 doi:10.20944/preprints202603.0128.v1

Quantitative rates derived from initial linear pH slopes (first 5 seconds) are presented in **Table 2** At 25°C, STM rates range from 1.0 to 1.4 × 10^{-13} mol·cm^{-2}·s^{-1}, consistent with literature values for crystalline, low-defect periclase [8]. In contrast, LBM rates under comparable conditions range from 3.3 × 10^{-9} to 7.7 × 10^{-8} mol·cm^{-2}·s^{-1}, representing enhancements of one to two orders of magnitude over STM rates, even after SSA normalization. This disparity persists at 35°C, where STM rates remain largely unchanged while LBM maintains elevated dissolution flux.

Table 2. Dissolution rates of LBM and analytical pure STM at 25°C and 35°C at near-neutral initial pH conditions (6.89 < pH < 8.01).

Temperature	Type	pH_0	slope: $2rS/V_R$	r (mol·cm^{-2}·s^{-1})	log r (mol·cm^{-2}·s^{-1})
25°C	STM	7.27	4.20E-08	1.40E-13	-12.85
		7.12	3.02E-08	1.00E-13	-13.00
		7.01	3.05E-08	1.02E-13	-12.99
	LBM	7.19	1.15E-06	3.84E-12	-11.42
		7.22	9.80E-08	3.26E-13	-12.49
		7.63	2.30E-06	7.67E-12	-11.12
		7.98	1.10E-06	3.67E-12	-11.44
35°C	STM	6.98	2.93E-08	9.77E-14	-13.01
		6.89	4.09E-08	1.36E-13	-12.87
		6.97	3.81E-08	1.27E-13	-12.90
	LBM	8.01	3.24E-07	2.00E-12	-11.72
		7.15	1.50E-06	9.29E-12	-11.03

The enhanced kinetics reflect the combined physicochemical characteristics identified in Section 3.1: smaller crystallite size and structural disorder providing higher reactive site density, textural porosity enabling water access to internal surfaces, and multiphase composition. While the 7.5 wt% CaO present as portlandite contributes to the measured pH evolution, particularly during initial contact with water, the equilibrium pH values (10.5-11.0) align with $Mg(OH)_2$ saturation rather than $Ca(OH)_2$ saturation (pH ~12.4), indicating that the overall dissolution process is governed by the more abundant MgO phase. The pH method thus captures the combined reactivity of LBM relevant to MBC applications, where both Mg^{2+} and Ca^{2+} participate in binding phase formation.

These findings have direct implications for MBC formulation. LBM's superior rates at neutral pH ensure efficient Mg^{2+} supply during early hydration, supporting binding phase formation. However, the enhanced kinetics also imply potential batch-to-batch variability from differences in calcination conditions or feedstock impurities, necessitating quality control protocols. The pH-monitoring method, validated against ICP-AES in Section 3.5, provides a practical tool for such characterization. This reference comparison demonstrates the method's capability to quantify material-dependent reactivity differences, setting the stage for examining LBM's pH-dependent dissolution behavior across the wider conditions relevant to MBC curing.

3.3. pH-Dependent Dissolution Mechanisms of LBM

The measured dissolution rates represent the combined behavior of all phases present in LBM. While portlandite (7.5 wt% CaO) has higher solubility than periclase and contributes to pH evolution, stoichiometric analysis indicates MgO dominates the overall signal. With 87.8 wt% MgO versus 7.5 wt% CaO (a 16.8:1 molar ratio), and observed equilibrium pH values (10.5-11.0, Figure 5) consistent

© 2026 by the author(s). Distributed under a Creative Commons CC BY license.

Preprints.org (www.preprints.org) | NOT PEER-REVIEWED | Posted: 2 March 2026 doi:10.20944/preprints202603.0128.v1

with $Mg(OH)_2$ rather than $Ca(OH)_2$ saturation (pH ~12.4), the measured kinetics primarily reflect MgO dissolution across the pH range investigated.

The solubility of MgO in aqueous solutions and its resultant dissolution rate are significantly modulated by the pH of the environment. In acidic conditions, solubility is markedly enhanced. The dissolution reaction in an acidic context can be represented by the following chemical equations:

$$Mg{-}OH^+ + H^+ \rightarrow Mg^{2+} + H_2O \quad (5)$$

$$MgO(s) + 2H^+(aq) \rightarrow Mg^{2+}(aq) + H_2O \quad (6)$$

These reactions delineate how MgO interacts with protons (H^+) in solution, yielding solvated magnesium ions and water molecules. The propensity of MgO to dissolve more readily at lower pH values is ascribed to the elevated concentration of H^+ ions [7,23]. At a pH below 5, the rate-determining step is proton attack, reliant on the concentration of H^+ and pre-existing Mg^{2+} in the solution; around pH 5, the process transitions to being diffusion-limited due to proton availability [8].

Conversely, at elevated pH levels, MgO's solubility decreases. It can undergo hydration, leading to the formation of magnesium hydroxide ($Mg(OH)_2$), which has a low solubility product and tends to precipitate from solution:

$$MgO + H_2O \rightarrow Mg(OH)_2 \quad (7)$$

Under highly alkaline conditions, magnesium hydroxide may further interact with hydroxide ions:

$$Mg(OH)_2 + 2OH^- \rightarrow Mg(OH)_4^{2-} \quad (8)$$

However, due to the low solubility product of $Mg(OH)_2$ ($K_{sp} = 5.61 \times 10^{-12}$) [21], it typically precipitates rather than forming soluble complexes. This precipitation can create passivating surface layers that dramatically reduce dissolution rates at pH > The rate-controlling step in alkaline conditions shifts to OH^- adsorption and subsequent Mg^{2+} and OH^- desorption, leading to complex kinetic behavior [8,24]. Furthermore, at pH levels exceeding 10, rapid dissolution of MgO nanocubes into $Mg(OH)_2$ nanosheets has been observed, demonstrating the dynamic nature of the dissolution-precipitation equilibrium [25].

The existing literature reveals that MgO powder dissolution rates are significantly higher than those of single crystals or natural periclase [6,8,9]. This enhancement cannot be explained by surface area differences alone, as these are typically normalized in rate calculations. Instead, factors such as crystallinity, surface defects, and the presence of impurities appear to play crucial roles [14–18]. For commercial LBM materials, the combined effects of these factors remain unquantified, representing a critical knowledge gap for MBC development.

Extending the near-neutral reference contrast from **Section 3.2**, where LBM's material properties drive superior kinetics, the full pH-dependent behavior of LBM at 25°C spans acidic to alkaline conditions (2.0-11.0) relevant to MBC hydration, with rates determined via the validated pH-monitoring method (detailed in **Section 2.4**) and compared to literature [7–10]. To ensure accuracy, the linearity of calculated proton or hydroxide consumption with respect to time was verified, confirming surface-controlled dissolution with constant reactive surface area (S) during the initial 5 seconds of reaction. **Figure 6** illustrates both this literature context and our experimental data, compiling reported dissolution rates from various studies [7–10] alongside LBM results, demonstrating the four-order-of-magnitude variability that limits predictive understanding.

© 2026 by the author(s). Distributed under a Creative Commons CC BY license.

Preprints.org (www.preprints.org) | NOT PEER-REVIEWED | Posted: 2 March 2026 doi:10.20944/preprints202603.0128.v1

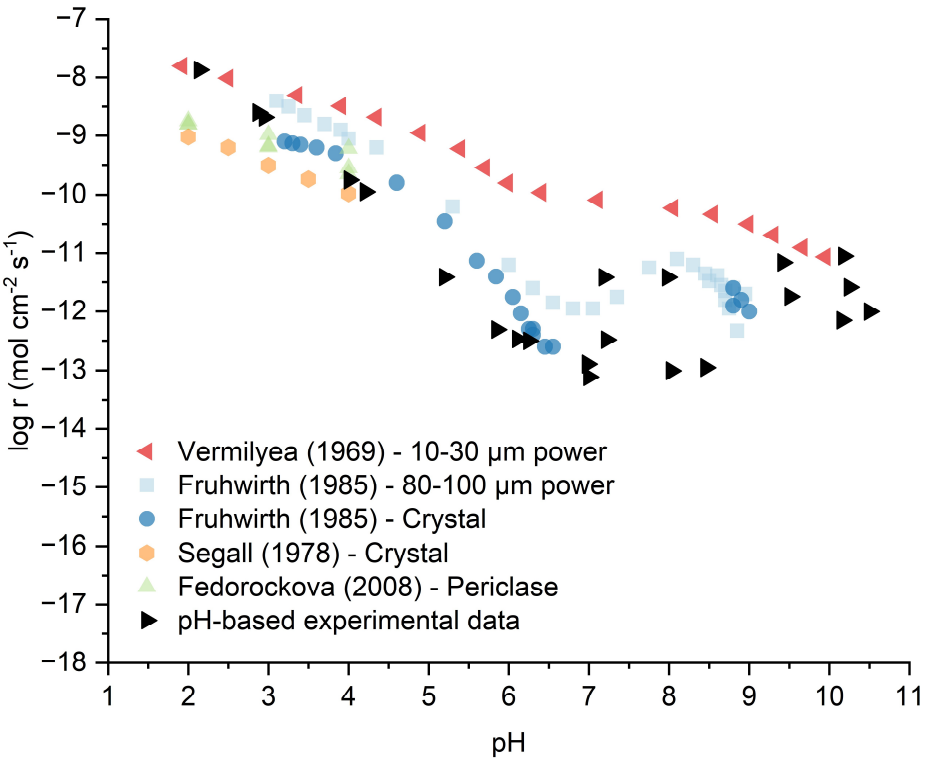

Figure 6. Relationship between the logarithm of the dissolution rate (log r) and pH for LBM at 25 °C, comparing the current pH-based dissolution rate data with data from previous literature: [6–9]. Rates are calculated from initial linear pH change during the first 5 seconds, representing surface-controlled dissolution before significant precipitation occurs at high pH. The form of MgO utilized is noted in the legend, which varied from natural periclase (MgO) to powderized forms (10-30 μm, and 80-100 μm) and single crystal with polished or cleaved surfaces. Experimental data available in supplementary information document.

As shown in **Figure 6**, under acidic conditions (pH 2.0–6.0), the logarithm of the dissolution rate (log r) exhibits a roughly linear relationship with pH. The linear trend shows a four-order-of-magnitude decrease in dissolution rate, similar to reported values in literature [6–9]. This confirms proton-promoted dissolution as the dominant mechanism, initiated by protonation of surface oxygen sites (>Mg-O$^-$ + H$^+$ → >Mg-OH), which weakens Mg-O bonds and facilitates Mg^{2+} release (Equations 5-6). The observed slope of approximately -1 indicates first-order dependence on proton activity [8,9], with LBM's enhanced rates stemming from its defect-rich structure.

The transition to near-neutral pH (6.0-9.0) marks a shift to pH-independent behavior, with rates fluctuating within one order of magnitude (-11.42 < log r < -12.49 mol/cm^2·s, or ~10^{-11} to 10^{-12} mol/cm^2·s). Notably, rates at pH 7.0-8.0 show elevation compared to adjacent pH values, a trend also observed in literature powder data [8]. This enhancement may result from transitional dissolution mechanisms or contributions from the multiphase composition identified in Section 3.1, particularly the presence of Ca-containing phases and textural porosity that provide continued water access to reactive sites. These effects are advantageous for MBC applications during the transition from neutral mixing to alkaline hydration environments.

Under alkaline conditions (pH >9.0), the measured dissolution behavior reflects the complex interplay between MgO dissolution and $Mg(OH)_2$ precipitation (Equation 7). The reported rates represent initial surface-controlled dissolution during the first 5 seconds before precipitation significantly affects the measured pH evolution. While pure MgO typically shows progressive passivation at high pH, the experimental data for LBM exhibit scatter spanning approximately one order of magnitude at pH 9-This variability likely arises from the combined dissolution of multiple phases in LBM (87.8 wt% MgO, 7.5 wt% CaO, plus silicates and carbonates identified in Section 3.1),

© 2026 by the author(s). Distributed under a Creative Commons CC BY license.

Preprints.org (www.preprints.org) | NOT PEER-REVIEWED | Posted: 2 March 2026 doi:10.20944/preprints202603.0128.v1

along with the influence of textural porosity and defect-rich crystallinity on local dissolution-precipitation equilibria. The pH-monitoring method provides practical reactivity assessment of initial reactivity across the full pH range (2.0-11.0) relevant to MBC hydration, though rates at pH >10 should be interpreted as composite material behavior rather than pure MgO kinetics.

3.4. Non-Monotonic Temperature Effects on LBM Dissolution Kinetics

This section examines the non-monotonic effects of temperature (25-85°C) on the dissolution kinetics of lightly burned magnesia (LBM), revealing a rate maximum at 75°C due to competing thermal activation and $Mg(OH)_2$ passivation processes. These are insights that build on the pH-dependent mechanisms in **Section 3.3** and offer practical guidance for optimizing magnesia-based cement (MBC) curing. While dissolution rates generally increase with temperature due to enhanced molecular kinetics [26–28], anomalous decreases occur at higher temperatures [29,30]. This anomalous behavior is attributed to enhanced $Mg(OH)_2$ precipitation at elevated temperatures, which creates more effective passivating layers [31,32]. Understanding these temperature effects is crucial for cement systems where exothermic reactions can raise temperatures.

Building on the pH-dependent mechanisms in **Section 3.3**, where dissolution transitions from proton-promoted to passivation-limited regimes, temperature introduces non-monotonic effects on LBM kinetics across pH 2.0-9.5, spanning conditions from ambient MBC hydration (40-60°C) to accelerated curing (up to 85°C). Rates were determined via pH monitoring (Equations 1-3), enabling continuous measurement of these thermal influences and providing practical guidance for optimizing MBC performance.

In the acidic regime (pH 2.0-4.0), dissolution rates are high (10^{-8} to 10^{-10} mol/cm²·s) and relatively independent of temperature, with clustered data showing limited systematic trends amid some scatter as in Figure This suggests that under high proton availability, the reaction is rapid, with thermal activation effects marginal compared to pH dominance. The near-neutral region (pH 5.0-8.0) shows more variable behavior, with rates at 75°C higher than at 25°C, reflecting transitional mechanisms such as impurity contributions as discussed in **Section 3.**Across the full range, rates at 85°C are lower than at 75°C, indicating a non-monotonic relationship with an apparent maximum at 75°C. This anomaly deviates from standard Arrhenius behavior due to competing processes: below 75°C, thermal activation enhances kinetics; above 75°C, accelerated $Mg(OH)_2$ precipitation (Equation 7) forms effective passivating layers[30,32].Equilibrium pH values support this, decreasing above 65°C (9.58-10.03 at 75°C vs. 9.04-9.66 at 85°C; see Supplementary Table S4 for raw data and processed ranges).

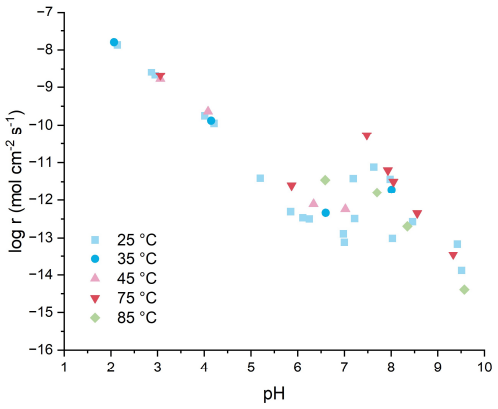

Figure 7. Effect of solution temperature (25-85°C) on the dissolution rate (log r) of LBM across various pH regimes (2.0 < pH < 9.5). Data available in supplementary information document.

© 2026 by the author(s). Distributed under a Creative Commons CC BY license.

Preprints.org (www.preprints.org) | NOT PEER-REVIEWED | Posted: 2 March 2026 doi:10.20944/preprints202603.0128.v1

In alkaline conditions (pH >8.0), temperature effects are minimal, with rates remaining relatively low across all temperatures, confirming that passivation dominates over thermal activation effects in this regime. The measured behavior aligns with literature observations showing reduced dissolution at high pH due to $Mg(OH)_2$ layer formation [9,32]. LBM's textural porosity may provide some continued water access to reactive sites even as external surfaces passivate, though high temperatures exacerbate layer formation.

These findings have direct implications for MBC development. The rate maximum at 75°C suggests optimal accelerated curing conditions to maximize early Mg^{2+} release and strength development [33,34], while avoiding 85°C where enhanced passivation may reduce reactivity. For ambient conditions (25°C), lower rates indicate the need for sufficient curing time or the use of activators in reactive LBM formulations. The pH-monitoring method enables such optimization under the exothermic conditions typical of MBC hydration, though future post-dissolution surface characterization could further refine understanding of passivation mechanisms.

3.5. Validation of the pH-Monitoring Method for Cement-Relevant Conditions

The temperature-dependent kinetics in **Section 3.4**, captured through continuous pH monitoring, underscore the need for reliable methods across diverse conditions—particularly alkaline regimes (pH >8-10) where MBC hydration occurs and traditional ion measurements falter due to rapid $Mg(OH)_2$ precipitation. To validate this stoichiometric pH approach (Equations 1-3) against direct Mg^{2+} quantification via ICP-AES (Equation 4), selected experiments at 25°C compared both techniques across pH 2.0-9.0, confirming its accuracy and practicality for cement-relevant studies.

As shown in **Figure 8**, the methods yield closely overlapping results in acidic conditions (pH 2.0-4.0), with dissolution rates (log r) agreeing within 0.5 log units. This close alignment affirms that proton consumption stoichiometry accurately tracks MgO dissolution under acidic conditions, validating pH monitoring as a reliable alternative to discrete ICP sampling in this regime.

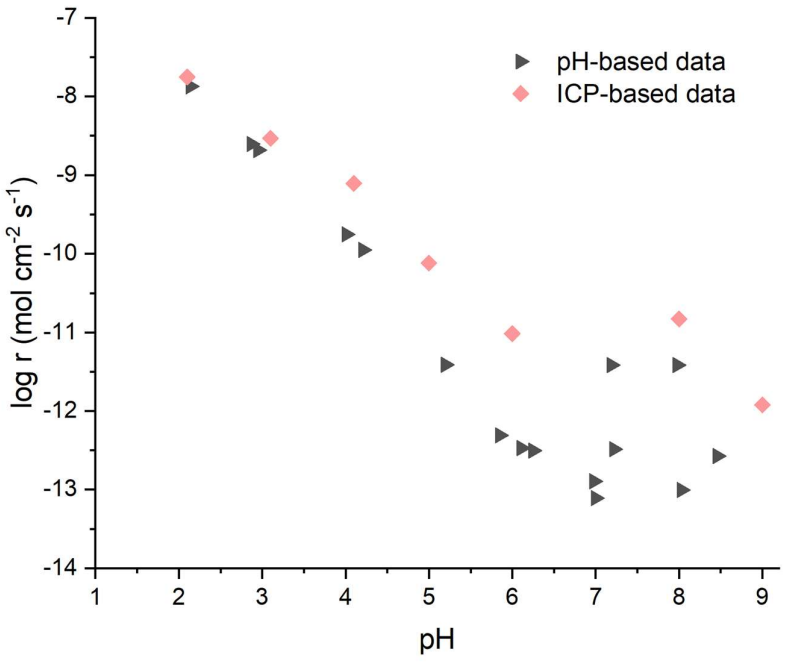

Figure 8. Comparison between both methodologies, namely the stoichiometric (pH) method and the aqueous chemical composition method, to determine the dissolution rate of LBM across varying pH regimes at 25 °C. Data available in supplementary information document.

© 2026 by the author(s). Distributed under a Creative Commons CC BY license.

Preprints.org (www.preprints.org) | NOT PEER-REVIEWED | Posted: 2 March 2026 doi:10.20944/preprints202603.0128.v1

At pH >4, ICP-derived rates become systematically higher than pH-based calculations, with the offset reaching approximately 0.5-1.5 orders of magnitude by pH 6-This divergence arises from the onset of $Mg(OH)_2$ precipitation. The pH method measures net hydroxide generation, reflecting the balance between MgO dissolution and $Mg(OH)_2$ precipitation, while ICP quantifies total dissolved Mg^{2+} concentrations, including ions that subsequently precipitate. As pH increases, a greater fraction of dissolved Mg^{2+} precipitates as $Mg(OH)_2$, reducing the net pH change relative to total Mg release. This explains why ICP consistently reports higher apparent dissolution rates than the pH method at pH >The validation experiments confirm that both methods capture dissolution behavior, but measure different aspects: ICP tracks cumulative Mg release while pH reflects net ion flux available for cement reactions.

Practically, pH monitoring offers continuous tracking without sampling artifacts, with sufficient sensitivity at high pH for real-time MBC hydration studies (pH 8-11) [3,35]. It addresses gaps in prior work by enabling reactivity assessment across the full pH spectrum relevant to cement applications. The validated methodology bridges experimental challenges in neutral and alkaline conditions, supporting systematic MBC investigations. Future work combining pH monitoring with post-dissolution surface characterization (e.g., SEM/XRD analysis of precipitated phases) could further elucidate the dissolution-precipitation mechanisms governing high-pH behavior.

4. Conclusions

This study provides a comprehensive investigation of commercial lightly burned magnesia (LBM) dissolution kinetics across pH 2.0–11.0 and temperatures 25–85°C, validating pH monitoring as a practical tool for tracking MgO consumption across conditions relevant to magnesia-based cements (MBCs). LBM exhibited rates one to two orders of magnitude higher than synthetic high-purity magnesia, ranging from 10^{-8} mol/cm²·s at pH 2 to 10^{-12} mol/cm²·s at pH 11, driven by poor crystallinity, multiphase composition (e.g., 7.5 wt% CaO as portlandite), and textural porosity (XRD/STEM/BET). Non-monotonic temperature effects, peaking at 75°C, arise from competing thermal activation and $Mg(OH)_2$ passivation, offering guidance for MBC curing protocols to optimize early strength while avoiding detrimental high-temperature effects. While focused on one commercial LBM, these findings highlight the need for standardized characterization to mitigate batch-to-batch variability in MBC performance.

The pH-dependent mechanisms transition from proton-promoted dissolution in acidic regimes (pH <6) to complex behavior in near-neutral conditions (pH 6-9), where rates are influenced by LBM's multiphase composition and textural porosity, and finally to passivation-dominated behavior in alkaline conditions (pH >9) where $Mg(OH)_2$ precipitation significantly affects measured kinetics. These mechanisms establish quantitative links between material characteristics and dissolution behavior essential for predictable MBC performance. The validated pH-monitoring method addresses prior gaps in alkaline studies by enabling continuous, artifact-free tracking across the full pH spectrum (2.0-11.0) encountered during cement hydration, supporting the development of reactive commercial LBM as a sustainable, low-carbon alternative to Portland cement.

This work has limitations, including the preliminary scope of synthetic magnesia comparisons (restricted to near-neutral pH) and absence of post-dissolution product characterization such as SEM/XRD of residues to confirm passivation mechanisms or assess LBM batch variability. These suggest avenues for future work, such as expanding comparative studies across the full pH range, analyzing precipitated phases to elucidate high-pH dissolution-precipitation dynamics, and testing LBM in blended MBC systems with supplementary cementitious materials to link dissolution kinetics to engineering performance metrics like compressive strength development and carbon footprint reduction. By providing a validated methodology for quantifying LBM reactivity, this work facilitates systematic optimization of MBC formulations toward economically viable and environmentally sustainable construction materials.

© 2026 by the author(s). Distributed under a Creative Commons CC BY license.

Preprints.org (www.preprints.org) | NOT PEER-REVIEWED | Posted: 2 March 2026 doi:10.20944/preprints202603.0128.v1

Supplementary Materials: The following supporting information can be downloaded at the website of this paper posted on Preprints.org.

Acknowledgments: This research was made possible by the Department of Architectural Engineering, the College of Engineering, and the D/Carb Group at the Pennsylvania State University. This research is dedicated to our late group member, Lovisa Arnesson-Cronhamre, who showed immense potential to be an excellent researcher. This work represents the views of the authors and not necessarily those of the sponsors.

Author Contributions: Conceptualization, Xiaowen Zhang and Juan Pablo Gevaudan; Methodology, Xiaowen Zhang; Formal analysis, Xiaowen Zhang; Investigation, Xiaowen Zhang; Writing – original draft, Xiaowen Zhang; Writing – review & editing, Xiaowen Zhang and Juan Pablo Gevaudan; Supervision, Juan Pablo Gevaudan; Project administration, Juan Pablo Gevaudan; Funding acquisition, Juan Pablo Gevaudan. All authors have read and agreed to the published version of the manuscript.

Funding: This research received no external funding.

Data Availability: The authors declare that the data supporting the findings of this study are available within the paper and its Supplementary Information files. Should any raw data files be needed in another format they are available from the corresponding author upon reasonable request.

Competing interests: The authors declare no competing interests.

References

1. J. Supriya, A. Raut, Performance Parameter Analysis of Magnesia Based Cement Products – A Review, IOP Conf. Ser.: Mater. Sci. Eng. 1197 (2021) 012078. https://doi.org/10.1088/1757-899X/1197/1/012078.
2. S.A. Walling, J.L. Provis, Magnesia-Based Cements: A Journey of 150 Years, and Cements for the Future?, Chem. Rev. 116 (2016) 4170–4204. https://doi.org/10.1021/acs.chemrev.5b00463.
3. T. Zhang, C.R. Cheeseman, L.J. Vandeperre, Development of low pH cement systems forming magnesium silicate hydrate (M-S-H), Cement and Concrete Research 41 (2011) 439–442. https://doi.org/10.1016/j.cemconres.2011.01.016.
4. M.G. Gardeh, A.A. Kistanov, H. Nguyen, H. Manzano, W. Cao, P. Kinnunen, Exploring Mechanisms of Hydration and Carbonation of MgO and Mg(OH)2 in Reactive Magnesium Oxide-Based Cements, J. Phys. Chem. C 126 (2022) 6196–6206. https://doi.org/10.1021/acs.jpcc.1c10590.
5. S. Ma, A.H. Akca, D. Esposito, S. Kawashima, Influence of aqueous carbonate species on hydration and carbonation of reactive MgO cement, Journal of CO2 Utilization 41 (2020) 101260. https://doi.org/10.1016/j.jcou.2020.101260.
6. R.L. Segall, R.St.C. Smart, P.S. Turner, Ionic oxides: distinction between mechanisms and surface roughening effects in the dissolution of magnesium oxide, J. Chem. Soc., Faraday Trans. 1 74 (1978) 2907. https://doi.org/10.1039/f19787402907.
7. A. Fedoročková, P. Raschman, Effects of pH and acid anions on the dissolution kinetics of MgO, Chemical Engineering Journal 143 (2008) 265–272. https://doi.org/10.1016/j.cej.2008.04.029.
8. O. Fruhwirth, G.W. Herzog, I. Hollerer, A. Rachetti, Dissolution and hydration kinetics of MgO, Surface Technology 24 (1985) 301–317. https://doi.org/10.1016/0376-4583(85)90080-9.
9. D.A. Vermilyea, The Dissolution of MgO and Mg (OH) 2 in Aqueous Solutions, J. Electrochem. Soc. 116 (1969) 1179. https://doi.org/10.1149/1.2412273.
10. S. Ruan, C. Unluer, Influence of supplementary cementitious materials on the performance and environmental impacts of reactive magnesia cement concrete, Journal of Cleaner Production 159 (2017) 62–73. https://doi.org/10.1016/j.jclepro.2017.05.044.
11. C. Unluer, A. Al-Tabbaa, The role of brucite, ground granulated blastfurnace slag, and magnesium silicates in the carbonation and performance of MgO cements, Construction and Building Materials 94 (2015) 629–643. https://doi.org/10.1016/j.conbuildmat.2015.07.105.
12. Calcinations Regulation Effect on Activity and Hydration of MgO from Magnesite Tailings | Scientific.Net, (n.d.). https://www.scientific.net/AMM.405-408.2559 (accessed August 25, 2024).

© 2026 by the author(s). Distributed under a Creative Commons CC BY license.

Preprints.org (www.preprints.org) | NOT PEER-REVIEWED | Posted: 2 March 2026 doi:10.20944/preprints202603.0128.v1

13. L. Mo, M. Deng, M. Tang, Effects of calcination condition on expansion property of MgO-type expansive agent used in cement-based materials, Cement and Concrete Research 40 (2010) 437–446. https://doi.org/10.1016/j.cemconres.2009.09.025.
14. R. Hacquart, J. Jupille, Morphology of MgO smoke crystallites upon etching in wet environment, Journal of Crystal Growth 311 (2009) 4598–4604. https://doi.org/10.1016/j.jcrysgro.2009.08.026.
15. G. PACCHIONI, QUANTUM CHEMISTRY OF OXIDE SURFACES: FROM CO CHEMISORPTION TO THE IDENTIFICATION OF THE STRUCTURE AND NATURE OF POINT DEFECTS ON MgO, Surface Review and Letters (2012). https://doi.org/10.1142/S0218625x00000336.
16. G. Jordan, S.R. Higgins, C.M. Eggleston, Dissolution of the periclase (001) surface; a scanning force microscope study, American Mineralogist 84 (1999) 144–151. https://doi.org/10.2138/am-1999-1-216.
17. N. Nilius, H.-J. Freund, Activating Nonreducible Oxides via Doping, Acc. Chem. Res. 48 (2015) 1532–1539. https://doi.org/10.1021/acs.accounts.5b00018.
18. M. Pettauer, A. Baldermann, S. Eder, M. Dietzel, Hydration of MgO: Reaction Kinetics and pH Control on Brucite Crystal Morphology, Crystal Growth & Design 24 (2024) 3085–3092. https://doi.org/10.1021/acs.cgd.4c00243.
19. J. Wang, H. Zhou, Y. Song, C. Xie, C. Unluer, S. Ruan, Revisiting MgO reactivity: The critical role of mesopores and surface defects of particles, Cement and Concrete Research 201 (2026) 108118. https://doi.org/10.1016/j.cemconres.2025.108118.
20. E. Bernard, H. Nguyen, S. Kawashima, B. Lothenbach, H. Manzano, J. Provis, A. Scott, C. Unluer, F. Winnefeld, P. Kinnunen, MgO-based cements – Current status and opportunities, RILEM Technical Letters 8 (2023) 65–78. https://doi.org/10.21809/rilemtechlett.2023.177.
21. C. Dong, G. He, W. Zheng, T. Bian, M. Li, D. Zhang, Study on antibacterial mechanism of Mg(OH)2 nanoparticles, Materials Letters 134 (2014) 286–289. https://doi.org/10.1016/j.matlet.2014.07.110.
22. O.S. Pokrovsky, J. Schott, Experimental study of brucite dissolution and precipitation in aqueous solutions: surface speciation and chemical affinity control, Geochimica et Cosmochimica Acta 68 (2004) 31–45. https://doi.org/10.1016/S0016-7037(03)00238-2.
23. P. Raschman, A. Fedoročková, Dissolution kinetics of periclase in dilute hydrochloric acid, Chemical Engineering Science 63 (2008) 576–586. https://doi.org/10.1016/j.ces.2007.10.004.
24. J.A. Mejias, A.J. Berry, K. Refson, D.G. Fraser, The kinetics and mechanism of MgO dissolution, Chemical Physics Letters 314 (1999) 558–563. https://doi.org/10.1016/S0009-2614(99)00909-4.
25. S.O. Baumann, J. Schneider, A. Sternig, D. Thomele, S. Stankic, T. Berger, H. Grönbeck, O. Diwald, Size Effects in MgO Cube Dissolution, Langmuir 31 (2015) 2770–2776. https://doi.org/10.1021/la504651v.
26. S.D. Rocha, M.B. Mansur, V.S. Ciminelli, Kinetics and mechanistic analysis of caustic magnesia hydration, Journal of Chemical Technology & Biotechnology 79 (2004) 816–821. https://doi.org/10.1002/jctb.1038.
27. W.H. Casey, G. Sposito, On the temperature dependence of mineral dissolution rates, Geochimica et Cosmochimica Acta 56 (1992) 3825–3830. https://doi.org/10.1016/0016-7037(92)90173-G.
28. N. Cohen, K.R. Westberg, Chemical kinetic data sheets for high-temperature chemical reactions, Journal of Physical and Chemical Reference Data 12 (1983) 531–590.
29. I. Lambert, H.L. Clever, Alkaline Earth Hydroxides in Water and Aqueous Solutions, Elsevier, 2013.
30. I. Lambert, A. Lefevre, J. Montel, 91-Gif-sur-Yvette (France) CEA Centre d'Etudes Nucleaires de Saclay, Solubility of magnesium hydroxide in aqueous solutions from 200 to 3000C. Influence of chlorides, CEA Centre d'Etudes Nucleaires de Saclay, 91 - Gif-sur-Yvette (France), 1982. https://inis.iaea.org/records/93dda-7ce94 (accessed July 17, 2025).
31. X. Tang, L. Guo, C. Chen, Q. Liu, T. Li, Y. Zhu, The analysis of magnesium oxide hydration in three-phase reaction system, Journal of Solid State Chemistry 213 (2014) 32–37. https://doi.org/10.1016/j.jssc.2014.01.036.
32. L.F. Amaral, I.R. Oliveira, R. Salomão, E. Frollini, V.C. Pandolfelli, Temperature and common-ion effect on magnesium oxide (MgO) hydration, Ceramics International 36 (2010) 1047–1054. https://doi.org/10.1016/j.ceramint.2009.12.009.
33. T. Zhang, J. Zou, B. Wang, Z. Wu, Y. Jia, C.R. Cheeseman, Characterization of Magnesium Silicate Hydrate (MSH) Gel Formed by Reacting MgO and Silica Fume, Materials (Basel) 11 (2018) 909. https://doi.org/10.3390/ma11060909.

© 2026 by the author(s). Distributed under a Creative Commons CC BY license.

Preprints.org (www.preprints.org) | NOT PEER-REVIEWED | Posted: 2 March 2026 doi:10.20944/preprints202603.0128.v1

34. N.T. Dung, C. Unluer, Advances in the hydration of reactive MgO cement blends incorporating different magnesium carbonates, Construction and Building Materials 294 (2021) 123573. https://doi.org/10.1016/j.conbuildmat.2021.123573.
35. Y. Liu, B. Wang, Y. Fan, J. Yu, T. Shi, Y. Zhou, Y. Song, G. Xu, C. Xiong, X. Zhou, Effects of reactive MgO on durability and microstructure of cement-based materials: Considering carbonation and pH value, Construction and Building Materials 426 (2024) 136216.

Disclaimer/Publisher's Note: The statements, opinions and data contained in all publications are solely those of the individual author(s) and contributor(s) and not of MDPI and/or the editor(s). MDPI and/or the editor(s) disclaim responsibility for any injury to people or property resulting from any ideas, methods, instructions or products referred to in the content.

© 2026 by the author(s). Distributed under a Creative Commons CC BY license.